# Solid Freeform Fabrication Based on Micro-Plasma Powder Deposition

Huijun Wang, Wenhui Jiang, Michael Valant and Radovan Kovacevic
Research Center for Advanced Manufacturing, Southern Methodist University
Richardson, TX 75081
Reviewed, accepted August 25, 2003

**Abstract**

This paper presents a solid freeform fabrication (SFF) technique based on micro-plasma powder deposition (MPPD). The relationship between the geometric features of the deposited layers and the welding parameters is investigated. The arc length is controlled through the monitoring of the arc voltage. The result of building parts with functionally graded components by the MPPD process is shown as well. The microstructure and the properties of the deposited layers are analyzed. The experimental results show that the MPPD process is a promising welding-based solid freeform fabrication technology.

## Introduction

Successfully responding to the ever changing and continually increasing high demands of today's global markets requires the rapid product development and manufacturing of new designs. Visualization tools often play a major role in taking an idea from the initial concept through the design phase, and into the final product development process. The following terms are often used interchangeably when referring to rapid prototyping technology: solid free-form fabrication, desktop manufacturing, layered manufacturing, and tool-less manufacturing. Solid freeform fabrication is one of the fastest growing automated manufacturing technologies that have significantly impacted the length of time between initial concept and actual part fabrication. However, to fully realize the potential cost and timesavings associated with rapid prototyping, the capacity to go from CAD models directly to metal components and tooling is crucial [1]. The use of arc welding to create freestanding shapes was established in Germany in the 1960's [2]. Companies such as Krupp, Thyssen, and Sulzer developed welding techniques for the fabrication of large components of simple geometry such as pressure vessels that can weigh up to 500 tons [3]. Other work in this area was undertaken by Babcock and Wilcox [4] who worked mainly on large components produced in an austenitic steel material. Also, work by Rolls-Royce has centered on investigating three-dimensional welding as a means of reducing the waste levels of expensive high-performance alloys that can occur in conventional processing. They have successfully produced various aircraft parts of nickel-based and titanium-based alloys. Research work on the welding-based rapid prototyping continues at universities and institutes such as the University of Nottingham, UK [5], the University of Minho, Portugal, the University of Wollongong, Australia [6-7], Southern Methodist University, USA [8-9], Korea Institute of Science and Technology and Hongik University [10], Indian Institute of Technology Bombay and Fraunhofer Institut Produktionstechnik und Automatisierung [11]. Most of the research work in this area is based on gas metal arc welding (GMAW) [3, 5, 6-8, 10] or gas tungsten arc welding (GTAW) [9].

The plasma arc technique is the only arc-welding process that is capable of achieving the energy density required for “keyhole” penetration - full penetration. However, high penetration keyhole welding is not the only capability of plasma arc welding. It can also be used as a low penetration weld surfacing technique. In this form it is commonly known as plasma transferred arc (PTA) surfacing or cladding. Being a modern advanced technology, PTA surfacing/cladding is widely used to coat details in high-risk functional areas with special materials that are resistant against intensive wear, corrosion, thermal, and percussive loading. Compared with conventional arc surfacing technologies, the PTA offers [12]:

1. A high deposition rate up to 10 kg/h;
2. A minimum losses of filler material;
3. A high quality of deposited metal;
4. A minimum penetration into the base metal (< 5%);
5. Deposits between 0,5 - 5,0 mm thickness and 3,0 - 50,0 mm width can be produced; rapidly in a single pass;
6. Fe-, Ni-, Co-, Cu- base alloys as well as composite materials can be clad.

In a competition with the laser surfacing/cladding, the PTA technology offers much higher productivity, a comparably higher quality of deposits and significantly lower costs. A PTA powder surfacing/cladding system (including power source, nozzle, and powder-feeding system) usually is about one-tenth the cost of a laser-based powder surfacing/cladding system.

In recent years, a number of researchers have paid more attention to the PTA surfacing/cladding technology. Matthes et al. [13-14] found that plasma-arc powder surfacing with the pulsed arc is a further development of shape welding that considerably reduces the thermal deformation of the component. The deformations and residual stresses caused on flat components by the intensive heat input during shape welding exert a negative influence on the component properties, particularly in the case of multi-pass weld surfacing. Dilthey et al. [15] developed a combined plasma-arc powder surfacing technique. It was a development from plasma-arc powder surfacing and plasma spraying. The advantages of the combined plasma-arc powder surfacing technique were less penetration depth and dilution, better mechanical properties of the surfacing weld, smaller heat-affect zone, and improvement in the possibility for isothermal heat input. Draugelates et al. [16-17] developed a plasma-arc powder nozzle and optimized the processing parameters with regard to heat input and powder delivery for the heavy-duty torch. It turned out that extensive coatings could be economically produced in one layer with dilution under 10%. They also implemented a two-powder plasma-arc surfacing process to manufacture anti-corrosion and anti-wear surfacing reinforced with oxide ceramics. So, plasma-arc-based deposition has been successfully used in cladding and surfacing. However, no literature has been found on the research topic – solid freeform fabrication based on plasma/micro-plasma powder deposition process. This paper investigates the feasibility of applying a micro-plasma powder deposition for solid freeform fabrication.

## Experimental set-up

Micro-plasma arc welding is a kind of plasma arc welding (PAW) using low current and a specially designed welding torch. PAW usually works in two basic methods: transferred and

non-transferred arc modes. A flowing plasma gas is provided through the center of the torch and exits through a copper nozzle. When an arc is established between the tungsten electrode positioned within the body of the torch and the copper nozzle, the gas is ionized, forming high-temperature plasma. The arc can be transferred to the workpiece where the intense heat causes fusion, and a weld is produced. With compression of the copper nozzle, the energy density of the micro-plasma arc becomes much higher, and the arc diameter and the HAZ become much smaller than that in a conventional welding arc such as a GTAW arc. So, micro-plasma welding applications often overlap with laser welding applications. The working principle of micro-plasma metal powder deposition is shown in Figure 1. A transferred plasma arc exists between the torch nozzle and the substrate, and generates a molten pool on the surface of the substrate. The metal powder is fed into the molten pool by the carrier gas (argon) through the powder feed nozzle. Then, the fed powder is melted under the high temperature of the plasma arc. With the moving away of the plasma arc, the molten metal solidifies to form a deposited layer.

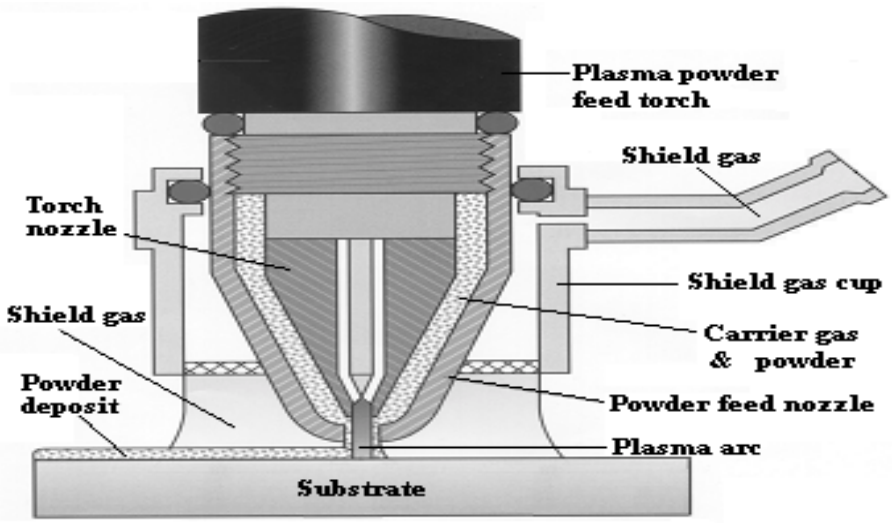


Fig. 1 Schematic diagram of micro-plasma powder deposition

The developed MPPD rapid prototyping system is shown in Figure 2. It consists of two axes in vertical position (Z axis and R axis), one axis in the horizontal position (X axis), two powder feeders, a powder feeder controller, a MPPD torch, a micro-plasma welding power source, a motion system controller, and a computer. The Z-axis is used to lift the welding torch up with the increase of the deposited wall during the deposition process. The three-dimensional part is built on a substrate that is fixed on a rotating axis, the R-axis. The R-axis is attached to the X-axis in the horizontal position. By controlling the movement of the X-axis in the depositing process, a part with a variable diameter can be obtained. The two powder feeders can be controlled at different powder feeding-rates, respectively. So, powders with different compositions can be deposited to build parts with functionally graded compositions.

## Substrate Preheating

Compared with the subsequent deposited layers, the first deposited layer has unique deposition conditions: the deposition base is the surface of a substrate (in this paper the dimensions of the

substrate are: outer diameter, 25 mm; inner diameter, 14 mm; height, 10 mm) at room temperature (25 °C). The subsequent layers are deposited on the surface of a previously deposited layer that is heated up to around 1000 °C. When a temperature gradient exists in a body, the heat energy is transferred by conduction. The heat-transfer rate per unit area is proportional to the normal temperature gradient:

$$q/A \sim \partial T / \partial x \quad (1)$$

where q is the heat-transfer rate, A is the section area perpendicular to the direction of the heat flow, and $\partial T/\partial x$ is the temperature gradient in the direction of the heat flow. When depositing the first layer, the temperature gradient between the welding-arc-heated area and the rest of the substrate is very large. The heat from the welding arc quickly dissipates into the substrate. So, it is difficult to accumulate enough energy to generate a molten pool on the surface of the substrate that is at room temperature. The status of the molten pool has a significant effect on the quality of the deposited layer. A smooth and uniform molten pool is the key for obtaining a deposited layer of high quality. One solution to the problem is to increase the initial temperature of the substrate before the starting of the deposition process. In this paper, the micro-plasma welding arc is used as a heat source to preheat the substrate. According to experimental results, the preheating parameters are determined as follows: welding current, 15 A; welding speed, 1 mm/s; and preheating time, 180 seconds.

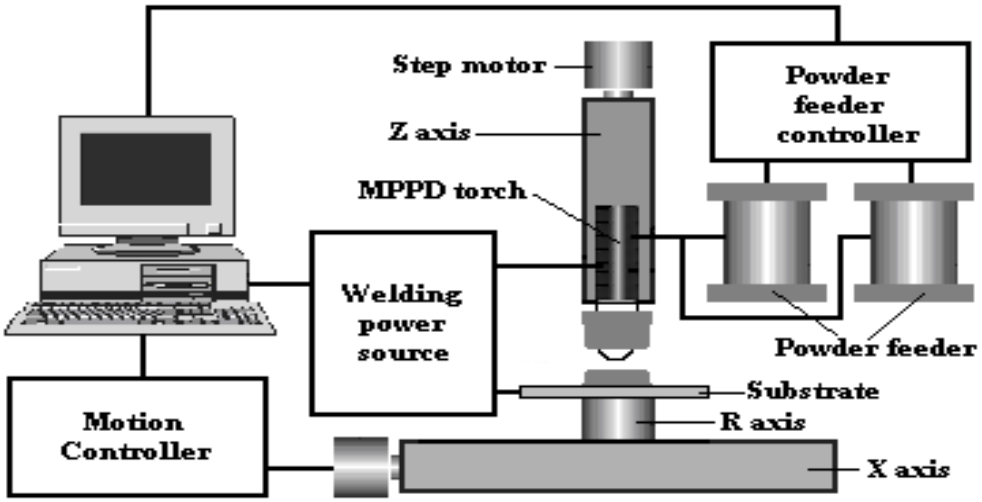


Fig. 2 Experimental Set-up for micro-plasma powder deposition

**Arc length control**

The arc length control is a key in the MPPD process. The reasons are as follows:

1. The heat input from the micro-plasma arc fluctuates with the variation of the arc length, and in turn, the molten pool size also fluctuates. The heat input from the welding arc Q is defined in Equation (2):

$$Q = \eta IV \quad (2)$$

where $\eta$ is the coefficient of efficiency, I is the welding current, and V is the arc voltage. The welding power source has a constant-current characteristic. The heat input is directly proportional to the arc length. So, a variation of the arc length causes a fluctuation in the arc voltage (V), and consequently, the heat-input (Q) varies as well. As well known, the heat input has a determinant effect on the molten pool size. So, a fluctuation of the arc length usually leads to an undesired variation of the molten pool size and in turn results in non-uniform deposited layers.

2. The arc length has an effect on the height of the deposited layer. In Figure 3, L1 and L2 denote arc length respectively and L1 is larger than L2. Assuming that except for the arc length all other parameters such as welding current, pilot gas flow rate, shielding gas flow rate, carrier gas flow rate, powder feeding speed, and traveling speed are the same in the two different cases, therefore the micro-plasma arc and the flowing behaviors of the carrier gas and the powder are the same. The shape of the feeding powder stream is shown in Figure 4. Laser strips are projected to the powder stream, and the reflection of the laser strips is recorded. It is seen that the shape of the powder stream is a cone. The shorter the distance between the nozzle and the cross section along the axis of the nozzle, the smaller the cross-section area. To simplify the analysis, assume that the distribution density of the powder is uniform on each cross section that is vertical to the axis of the nozzle. According to the law of conservation of mass, the smaller the cross-sectional area of the carrier-gas and powder flow, the larger the distribution density of the powder. So per unit area of the molten pool, much more powder is received at arc length L2 than at arc length L1. Because the height of the deposited layer is directly proportional to the amount of the fed powder on the molten pool per unit area, a larger height of the deposited layer is generated when the arc length is short.

In order to monitor and control the arc length in the MPPD process, the relationship between the arc length and the arc voltage is investigated. For instance, when the current is 15 A, the relationship between the arc length and the arc voltage is shown in Figure 5. It is seen that the arc voltage has a linear relationship with the arc length when the current is constant. The arc voltage is directly proportional to the arc length. In addition according to the experimental results, it is also noted that the current has an effect on the relationship between the arc voltage, and the arc length and the effect of current is nonlinear and complicated. So, an arc length control strategy is developed based on the real-time measurement of the arc voltage and current:

1. The arc voltage is acquired at selected arc lengths and currents. The selected arc lengths are from 1 mm to 6 mm with an increment of 0.5 mm. The selected currents are from 10 A to 15 A with an increment of 1 A.
2. Five linear equations can be obtained by linear regression analyses of the data acquired at different currents. Each linear equation describes the relationship of the arc voltage and the arc length at a corresponding current.
3. In the MPPD process, the current is always set to be one of the selected current values (10 A, 11 A, 12 A, 13 A, 14 A, and 15 A). The current is constant after it is set because the power supply has a characteristic of constant-current output. So, the effect of current fluctuation on the relationship of the arc voltage and arc length can be neglected. The arc length control process consists of the following steps: acquiring arc voltage, low-pass filtering of the acquired signal, selecting a linear equation according to the current value, calculating the arc length, and moving the torch 0.05 mm up (down) if the calculating result is smaller (larger) than the given arc length. Repeat the process.

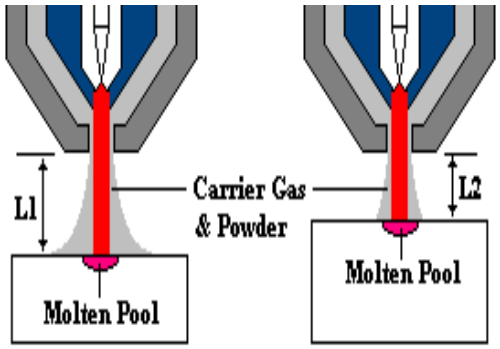


Fig. 3 Effect of arc length on powder feeding

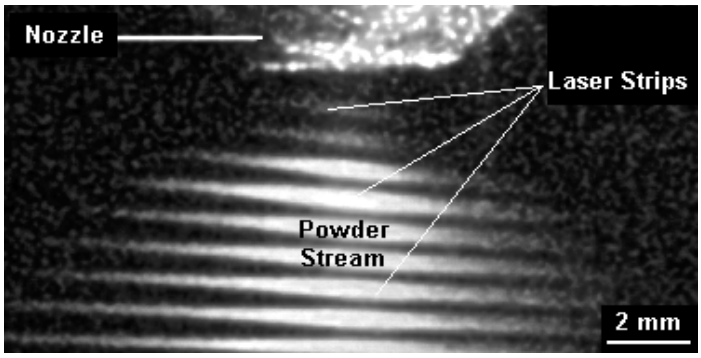


Fig. 4 Shape of the feeding powder stream

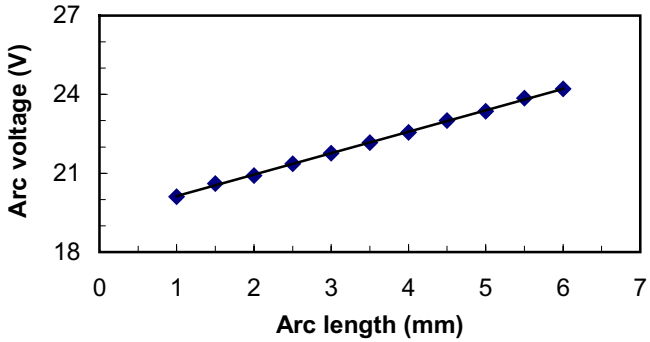


Fig. 5 Relationship between arc length and arc voltage at 15-A current

**Relationship between welding parameters and deposited layer's geometry**

The effect of the welding speed on the deposited layer's geometries is shown in Figure 6(a). The welding speed is 3.14 mm/s, 4.18 mm/s, and 6.28 mm/s, respectively. The welding current is 15 A, the arc length is 3.0 mm, the plasma gas flow rate is 0.4 l/min, the shielding gas flow rate is 10 l/min, and the powder-carrier gas flow rate is 3.5 l/min. The powder is H13 tool steel, and the powder-feeding rate is 2.3 g/min. It is seen that both of the deposited layer's width and height decrease with the increase in the welding speed. The effects of the welding speed on the width and height of the deposited layer are almost the same. The effect of the welding current on the deposited layer's geometry is shown in Figure 6(b). The welding current is 15 A, 13 A, and 11 A, respectively. The welding speed is 3.14 mm/s, the arc length is 3.0 mm, the plasma gas flow rate is 0.4 l/min, the shielding gas flow rate is 10 l/min, and the powder-carrier gas flow rate is 3.5 l/min. The powder is H13 tool steel and the powder-feeding rate is 2.3 g/min. It is seen that the width of the deposited layer increases with the increase in the welding current. The height of the deposited layer decreases slightly with the increase in the welding current. The effect of the powder-feeding rate on the deposited layer's geometries is shown in Figure 6(c). The powder is H13 tool steel, and the powder-feeding rate is 1.2 g/min, 2.3 g/min, and 3.6 g/min, respectively. The welding current is 15 A, the arc length is 3.0 mm, the plasma gas flow rate is 0.4 l/min, the shielding gas flow rate is 10 l/min, and the powder-carrier gas flow rate is 3.5 l/min. It is seen that the deposited layer's height increases with the increase in the powder-feeding rate. The deposited layer's width slightly decreases with the increase in the powder-feeding rate. It is also seen that the powder-feeding rate has a much larger influence on the height of the deposited layer than on the width of the deposited layer.

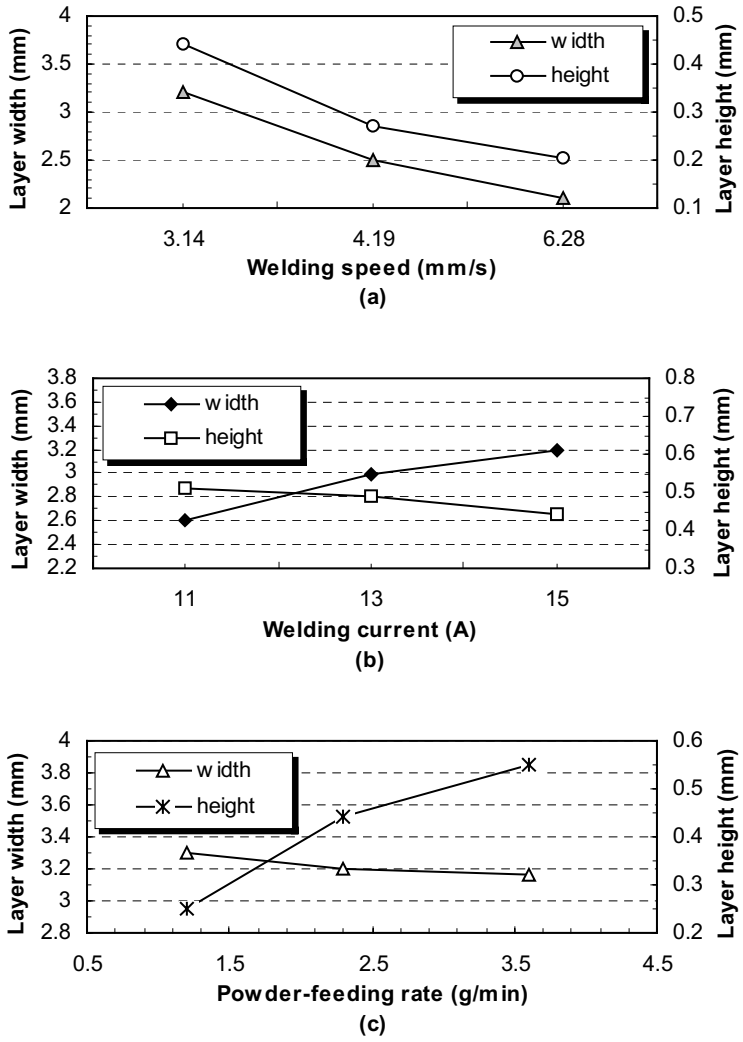


Fig. 6 Effects of welding parameters on the geometries of the deposited layer: (a) effect of welding speed; (b) effect of welding current; (c) effect of powder-feeding rate

## Test parts

Several test parts are built with the developed MPPD process as shown in Figure 7. The geometrical parameters of the part in the form of a cylinder [Figure 7(a)] are as follows: number of layers is 80; the average layer of thickness is about 0.42 mm; the outer diameter is 22.4 mm; and the inner diameter is 17.2 mm. The geometrical parameters of the part in form of a cone [Figure 7(b)] are as follows: number of layers is 40; the average layer of thickness is about 0.35 mm; the outer diameter at the top is 30.0 mm; the inner diameter at the top is 26.2 mm; the outer diameter at the bottom is 21.5 mm; the inner diameter at the bottom is 16.5 mm; and the over-hang angle is 23 degree. The test part in the form of a cylinder, as shown in Figure 7(a), is deposited with 80 layers. The traveling speed is 3.14 mm/s. The diameter of the deposited part is 20 mm. The powder-feeding rate is 2.3 g/min. So, the amount of feeding powder in the deposition process is 61.3 g. The weight of the substrate is 28.9 g. After the deposition process,

the total weight of the substrate and the deposited cylinder part is 65.1 g. So, the powder utilization efficiency in this deposition process is about 59%.


(a) (b)

Fig. 7 Test parts: (a) part in form of a cylinder; (b) part in form of a cone

The term functionally graded composition (FGC) is applied to components whose composition and structure vary progressively as a function of position. A FGC (along the z-axis) test part is produced by the successive deposition of the H13 tool steel powder and tungsten carbide powder. The part is in the form of a cylinder (the height, 6 mm; the outer diameter, 23.0 mm; and the inner diameter, 17.5 mm) and is built with 20 layers on a mild-steel substrate. The cross section of the FGC part is shown in Figure 8. In the first 12 layers, the feeding powder is 100% H13 tool steel powder. From layer 13, the tungsten carbide powder is blended with H13 tool steel. The percentage of volume of the tungsten carbide powder increases gradually from 0 to 20 %. Figure 9 shows the interface between the substrate and the deposited wall that corresponds to position A in Figure 8.

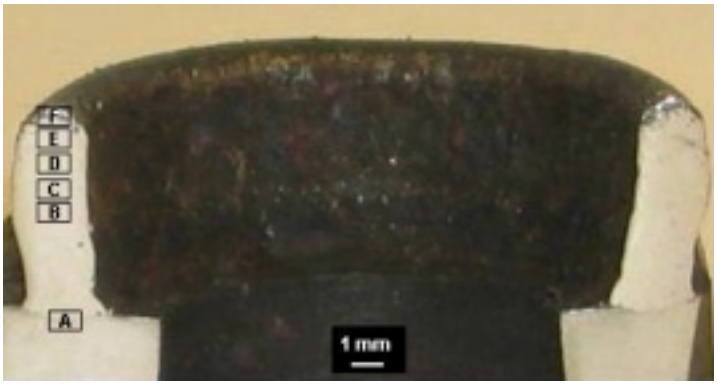


Fig. 8 Cross section of a FGM test part

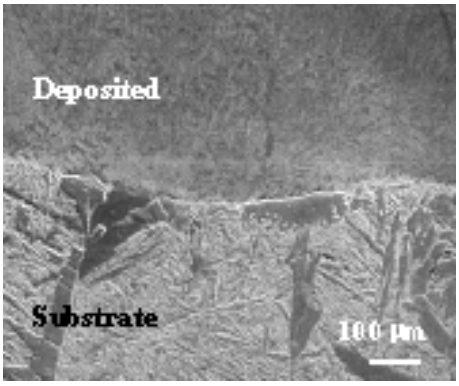


Fig. 9 Interface between the substrate and the deposited wall

Scanning electron microscopy (SEM) observation indicates that injected tungsten carbide dissolves and subsequently, fine carbides precipitate from supersaturated melt during cooling, as shown in Figure 10. The dissolution of tungsten carbide is rather aggressive during deposition. Only at the top of the part can injected coarse tungsten carbide be observed, as shown in Figure 11. The reprecipitation of fine carbide happens extensively. Its morphology, size, and amount are closely related to the amount of injected tungsten carbide. Figure 12 shows typical microstructures of reprecipitated carbide that correspond to the positions B, C, D, and E in Figure 8. In these back-scattered electron images, the precipitated carbide appears brighter than the matrix, indicating that it is rich in tungsten. At the lowest amount of injected tungsten carbide, the precipitated carbide is fewer, globular, and located at the grain boundary of the matrix [Figure 12(a)]. By increasing the injected tungsten carbides, the amount of precipitated carbide increases and its morphology evolves into an intergranular network [Figure 12(b)]. The higher amount of injected tungsten carbide results in the formation of herringbone [Figure 12(c) and (d)]. At a higher magnification, a significant amount of dark carbide can be seen [Figure 13]. It may be MC rich in titanium and chromium, whose contents in H13 are as high as 5.2 and 4.3 wt.%, respectively.

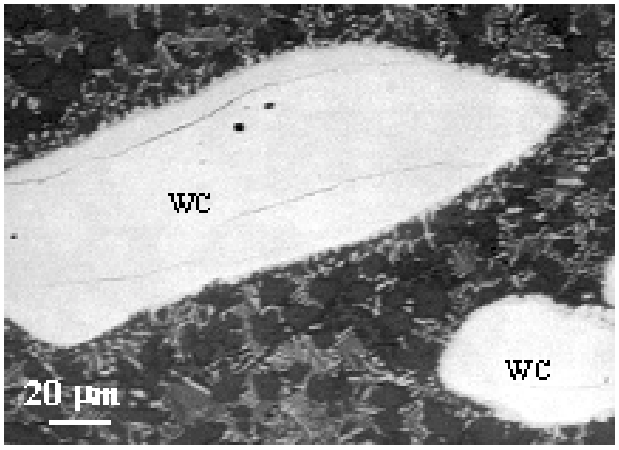


Fig. 10 Dissolution of tungsten carbide and Precipitation of fine carbides
(WC – tungsten carbide)

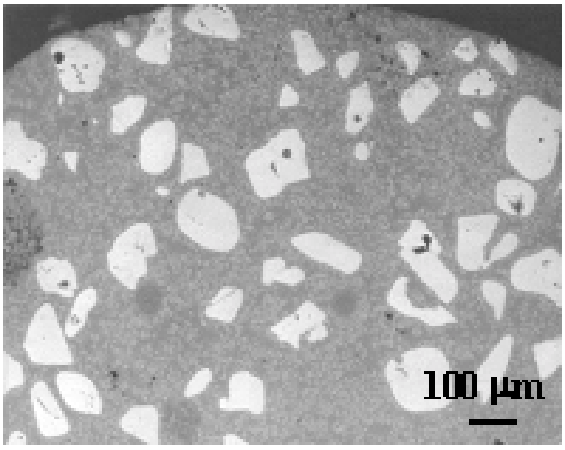


Fig. 11 Coarse tungsten carbide on top layers of the FGM part

Microstructural observation indicates that tungsten carbide is unstable and dissolves during deposition. Injected coarse tungsten carbide is observed only at the top of the deposited part. This result may be attributed to rapid cooling and a higher amount of injected tungsten carbide. Dissolution of injected tungsten carbide increases the contents of tungsten and carbon in the melt. During subsequent cooling, tungsten carbide precipitates from the supersaturated melt. From the present metallographical observation, it can be inferred that a eutectic reaction is predominant during solidification. When the amount of injected tungsten carbide is smaller, and consequently, fewer tungsten and carbon atoms are released into the melt, the melt is hypoeutectic and tungsten carbide precipitates as a final formed phase and is pushed to the grain boundary of the matrix. A higher amount of injected tungsten carbide increases the contents of tungsten and carbon in the melt. That increase results in a eutectic reaction during solidification, forming herringbone carbide.

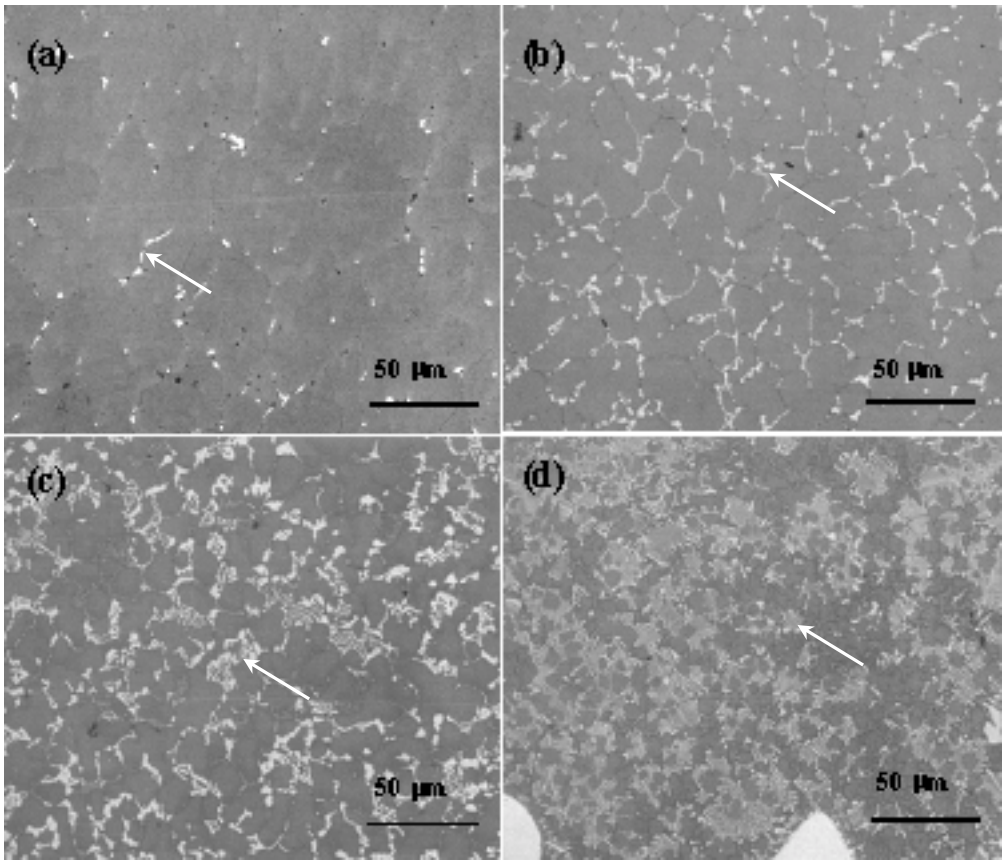


Fig. 12 Microstructures of re-precipitated carbide corresponding to the position in Fig.8: (a) position B; (b) position C; (c) position D; (d) position E. (the arrow indicates the phases

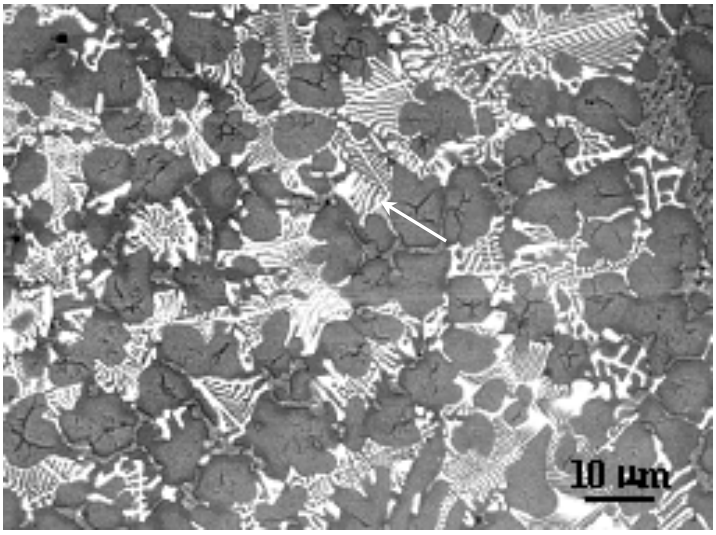


Fig. 13 Microstructures of re-precipitated carbide at a higher magnification (the arrow indicates the phases)

The Vickers hardness (HV) distribution along the cross section of the test FGC part is shown in Figure 14. It is seen that the hardness of the deposited wall continuously increases by increasing the amount of injected tungsten carbide. The hardness value is an average value at three different points in the same testing area. The hardness of the tungsten carbide is 1114 Hv.

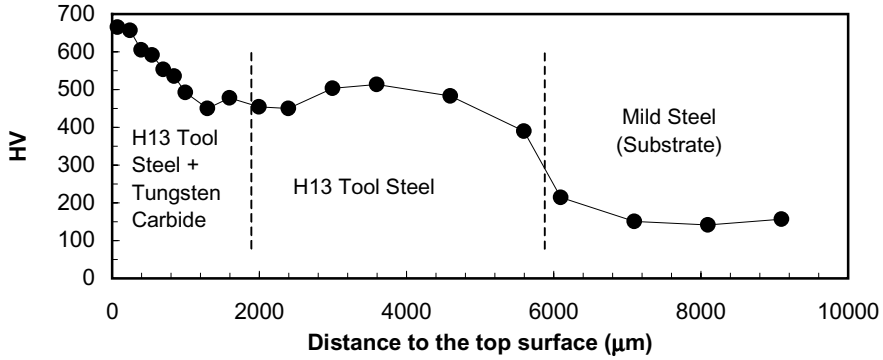


Fig. 14 Hardness (HV) distribution on the cross section of the test FGM part

## Conclusions

The MPPD based SFF process allows the components to be directly built from the corresponding powder. Substrate preheating and arc length control are required in the developed deposition process. The arc voltage signal can be used to monitor and control the arc length according to the developed control strategy. The power of the micro-plasma arc applied in the deposition process is less than 375 W. A number test parts are made of H13 tool steel powder with acceptable surface quality and mechanical properties including parts with functionally graded composition. The powder utilization efficiency is about 59%. The microstructural observation on the FGC part shows that the dissolution of tungsten carbide is fast occurring during deposition. Injected coarse tungsten carbide can only be observed at the top of the part. The reprecipitation of fine carbide happens extensively. From the metallographical observations, it can be inferred that a eutectic reaction is predominant during solidification. Experimental result shows that the hardness of the built FGC part continuously increases with increase in the amount of injected tungsten carbide.

## Acknowledgement

The work was financially supported by U.S. Department of Education Grant No. P200A80806-98 and THECB's Grant No. 003613-0016-2001.

## Reference

1. J. J. Beaman, J. W. Barlow, R. H. Bourell, H. L. Craford, H. L. Marcus and K. P. McAlea, “Solid Freeform Fabrication: A New Development in Manufacturing,” Kluwer Academic Publishers, Dordrecht/Boston/London, 1997.
2. K. Kassmaul, F. W. Schoch, and H. Lucknow, "High Quality Large Components "Shape Welded" by a SAW Process", September 1983, Welding Journal.

3. K-H. Piehl, "Formgebendes Schweiβen von Schwekomponenten", January 1989, Company report: Thyssen Aktiengesellschaft, Duisburg.
4. T. E. Doyle, (Babcock & Wilcox), "Shape Melting Technology", October 1991, The Third International Conference on Desktop Manufacturing: Making Rapid Prototyping Pay Back, The Management Round Table.
5. P. M. Dickens, R. Cobb, I. Gibson, and M.S. Pridham, "Rapid Prototyping Using 3D Welding," Journal of Design and Manufacturing, No.3, 1993.
6. A. F. Ribeiro and J. Norrish, " Metal Based Rapid Prototyping for More Complex Shapes", 6th Biennial International Conference on "Computer Technology in Welding", TWI, Abington Publishing, 9-12 June 1996, Lanaken, Belgium.
7. A. F. Ribeiro and J. Norrish, " Rapid Prototyping Process Using Metal Directly", Proc. of the 7th Annual Solid Freeform Fabrication Symposium, Aug. 12-14, 1996, Austin, TX.
8. R. Kovacevic and H. E. Beardsley, "Process Control of 3D Welding as a Droplet-Based Rapid Prototyping Technique", Proc. of the 9th Annual Solid Freeform Fabrication Symposium, Aug. 10-12, 1998, Austin, TX
9. H. Wang and R. Kovacevic, "Rapid Prototyping Based on Variable Polarity Gas Tungsten Arc Welding for 5356 Aluminum Alloys", the Proceedings of the Institution of Mechanical Engineers, Part B, Journal of Engineering Manufacture, Vol. 215, November, 2001, pp. 1519-1527.
10. Y. Song, S. Park, K, Hwang, D. Choi and H. Jee, "3D Welding and Milling for Direct Prototyping of Metallic Parts", Proc. of the 9th Annual Solid Freeform Fabrication Symposium, Aug. 10-12, 1998, Austin, TX
11. K. Karunakaran, P. Shanmuganathan, S. Roth-Koch and U. Koch, "Direct Rapid Prototyping of Tools", Proc. of the 9th Annual Solid Freeform Fabrication Symposium, Aug. 10-12, 1998, Austin, TX
12. http://www.plasma-master.com.ua/eng/science/science_pta.htm
13. K.-J. Matthes, K. Alaluss and F. Khaled, "Utilisation of the Finite-element Method in Order to Optimize Shaping Plasma-arc Powder Weld Surfacing for the Manufacture of Forming Tools Suitable for High Stresses", Schweissen und Schneiden/Welding and Cutting, Vol. 54, No. 3, 2002, pp. 165-169.
14. K.-J. Matthes and K. Alaluss, "Plasma-arc Powder Surfacing with Pulsed Arc for Minimum Deformation Shaping", Schweissen und Schneiden/Welding & Cutting, Vol. 48, No. 9, Sep, 1996, pp. E170-E172.
15. U. Dilthey, J. Ellermeier, P. Gladkij and A. V. Pavlenko, "Combined plasma-arc powder surfacing", Schweissen und Schneiden/Welding and Cutting, Vol. 45, No. 5, May, 1993, pp. E75-E76.
16. U. Draugelates, B. Bouaifi and S. Giessler, "Two-powder Plasma-arc Surfacing of Nickel-base Alloys Containing Oxide Ceramics", Schweissen und Schneiden/Welding & Cutting, Vol. 50, No. 11, Nov, 1998, pp. 217-218.
17. U. Draugelates, B. Bouaifi and S. Schultze, "Heavy-duty Plasma-arc Powder Surfacing with Duplex Steels", Schweissen und Schneiden/Welding and Cutting, Vol. 51, No. 5, May, 1999, pp. E77-E81.